Journal of Materials Chemistry A

ROYAL SOCIETY OF CHEMISTRY

PAPER

View Article Online
View Journal | View Issue

Cite this: J. Mater. Chem. A, 2022, 10, 6073

High-loading metal atoms on graphdiyne for efficient nitrogen fixation to ammonia†

Yan Fang,[ac] Yurui Xue,*[ab] Lan Hui,[ac] Xi Chen[ac] and Yuliang Li *[ac]

Received 24th September 2021
Accepted 2nd November 2021

DOI: 10.1039/d1ta08241h

rsc.li/materials-a

Atomic catalysts have shown great potential in the field of catalysis because of their maximum atomic utilization, and high reaction selectivity and activity. Graphdiyne-based atomic catalysts have emerged as a new class of promising materials in catalysis. Here, a new graphdiyne-based manganese atomic electrocatalyst (Mn_{SA}/GDY) was designed and successfully synthesized *via* a facile *in situ* reduction strategy for electrochemical nitrogen fixation to ammonia. Experimental results reveal that single Mn atoms were successfully anchored and highly dispersed on the surface of GDY, forming a catalyst with a determined chemical structure, facilitated charge transfer capability and maximized active sites. These special characteristics provide Mn_{SA}/GDY with a high ammonia yield rate (up to 46.78 μg h^{-1} $mg_{cat.}^{-1}$) and faradaic efficiency (39.83%), as well as cycling durability, which outperform those of most reported conventional atomic electrocatalysts and heterostructured ones. This work broadens the application scope of GDY-based atomic catalysts and demonstrates their applicability in the field of energy conversion.

Introduction

The ammonia industry has undergone tremendous development since its inception and has greatly changed the landscape of our planet; its impact on our daily life is enormous. Ammonia has been widely used to produce synthetic nitrogen fertilizers that are essential for crop harvesting.[1–3] Additionally, it has been used for producing numerous chemical compounds (*e.g.*, urea, ammonium nitrates, ammonium phosphates, and other nitrogen compounds) and industrial refrigerants. Today, more than 90% of ammonia is synthesized through the Haber–Bosch process,[4] which requires high-purity N_2 and H_2 and high temperature and pressure, thereby inducing harmful effects on the environment from a long-term perspective because of its fossil-fuel-dependent and energy-intensive features. Considering that the human-induced energy crisis and climate change have aroused international concerns, scientists have devoted tremendous efforts to explore innovative approaches for ammonia synthesis with the aim of reducing the energy consumption and CO_2 emissions from the current industrial ammonia synthesis process.[5]

Given that the cost of electricity generation has shown a decreasing trend annually, the electrocatalytic nitrogen reduction reaction (ECNRR) powered by electricity generated from solar or wind sources has been considered as a promising and economically viable alternative approach for ammonia synthesis.[4,6,7] The ECNRR can be performed at ambient temperature and pressure in relatively small-scale, distributed, and on-site electrolysis cells. However, a critical research issue is the exploration of efficient electrocatalysts to break the inert molecular structure of N_2, which has a high triple bond energy of 941 kJ mol^{-1}, and facilitate subsequent delivery and transfer of protons and electrons.[6] Another major issue for ECNRR research is that the competitive hydrogen evolution reaction which limits the faradaic efficiency and leads to a low overall reaction rate should be hindered by electrocatalysts with high selectivity for nitrogen fixation and reduction. Fragile molecular-scale catalysts do not meet the requirements of long-term electrocatalysis, although they possess good NH_3 selectivity.[4] The challenges presented by fragile molecular-scale catalysts can be circumvented by using heterogeneous electrocatalysts.[8] Numerous studies have reported achieving great improvements in electrocatalytic activity, stability, and selectivity when using various heterogeneous electrocatalysts containing noble metals (Au, Ru, Pd, and Pt) and their alloys,[9,10] transition metals (Fe, Mo, Cu, and V) and their alloys,[11] nitrides,[12] oxides,[11] sulfides,[13–17] and metal-free catalysts.[18–20] Compared with the above-mentioned electrocatalysts, research on atomic catalysts with higher atomic utilization and cost-effectiveness appears to be scarce.

Graphdiyne (GDY), a novel two-dimensional carbon allotrope in which adjacent sp^2-hybridized benzene rings are linked to each other *via* sp-hybridized butadiyne linkages, features a highly conjugated system with strong reduction ability, an

[a]Institute of Chemistry, Chinese Academy of Sciences, Beijing, 100190, P. R. China. E-mail: ylli@iccas.ac.cn

[b]Science Center for Material Creation and Energy Conversion, Institute of Frontier and Interdisciplinary Science, School of Chemistry and Chemical Engineering, Shandong University, Jinan 250100, P. R. China. E-mail: yrxue@sdu.edu.cn

[c]University of Chinese Academy of Sciences, Beijing 100049, P. R. China

† Electronic supplementary information (ESI) available. See DOI: 10.1039/d1ta08241h

intrinsic uniform porous structure and excellent mechanical properties.[21–23] It has been widely applied in various research fields, including catalysis, batteries, solar cells, and electrochemical actuators owing to its fascinating properties.[24–29] It is worth noting that the arbitrary angle of rotation (π/π^*) perpendicular to the axis in the GDY structure enables it to chelate single metal atoms, thereby making it possible to use it as an ideal support for anchoring and preparing atom catalysts without any pre-treatment.[24] Many GDY-based atomic electrocatalysts have been successfully synthesized and demonstrated excellent activities towards various catalytic reactions.[24,30–33] Additionally, theoretical investigations of single and double transition metals (Fe, Mn, Nb, Cr, V, *etc.*) anchored on graphdiyne for nitrogen reduction reactions have recently demonstrated good catalytic activity and selectivity in nitrogen fixation under ambient conditions.[34,35] This outcome has inspired the current study with an aim of widening the application space of GDY-based atomic catalysts in the field of electrochemical ammonia synthesis. Therefore, this study demonstrates the first successful preparation of manganese atomic electrocatalysts anchored on the GDY substrate (Mn_{SA}/GDY) and their promising properties in electrocatalytic nitrogen reduction reactions.

Results and discussions

The freestanding Mn_{SA}/GDY catalytic electrode was prepared *via* a facile two-step strategy involving the initial synthesis of GDY nanosheets (GDY NSs) on nitric acid-treated carbon cloth *via* an acetylenic cross-coupling reaction. This step was followed by *in situ* anchoring of Mn atoms on GDY NSs through electrochemical reduction deposition at an overall mass loading of 0.155 mg cm^{-2} (Fig. 1a). Scanning electron microscopy (SEM) images (Fig. 1b–d) revealed the porous and ultrathin nanosheet morphology of the as-prepared GDY and Mn_{SA}/GDY, respectively. Inductively coupled plasma mass spectrometry (ICP-MS) analysis suggested that the mass loading of Mn atoms on GDY NSs was 0.19 wt%. The contact angle measurement results (Fig. 1e) indicated the hydrophilicity of the Mn_{SA}/GDY surface, which could reduce the contact and transport resistance between the aqueous electrolyte and electrode, thereby facilitating the subsequent electrochemical reaction. Transmission electron microscopy (TEM) was conducted for the morphological characterization of porous Mn_{SA}/GDY (Fig. 2a). High-resolution transmission electron microscopy (HRTEM) images only showed the interplanar distance of GDY without any lattice fringe of the metal species (Fig. 2b and c). Subsequent high-angle annular dark-field scanning transmission electron microscopy (HAADF-STEM) images revealed the isolated and uniform dispersion of bright dots representing heavy-element atoms. This result confirmed the successful anchoring of Mn atoms on GDY (Fig. 2d–h). In addition, scanning TEM (STEM) and corresponding elemental mapping results indicated the presence of C and Mn elements (Fig. 2i).

Raman spectroscopy, X-ray diffraction (XRD) analysis and X-ray photoelectron spectroscopy (XPS) were also performed to investigate the chemical composition and structure of Mn_{SA}/GDY. The XRD spectra of both Mn_{SA}/GDY and GDY (Fig. 3a) showed only the characteristic peaks of carbon. Raman spectra of pure GDY and Mn_{SA}/GDY (Fig. 3b) both suggested the typical D and G bands of carbon materials and peaks attributed to the vibration of conjugated diyne units (C≡C, peaks marked with "*") of GDY.[21] In contrast, the higher intensity ratio of D/G of Mn_{SA}/GDY than that of pure GDY implied its more defective property and the abundance of electrocatalytically active sites. XPS measurements were performed to explore the valence state and chemical bonding of the samples. The valence band spectra in Fig. 3d exhibited the variation trend of valence band maxima

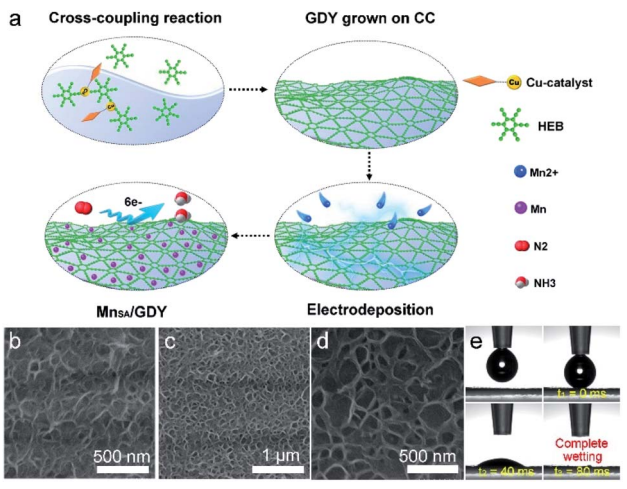

Fig. 1 (a) Schematic representation of the synthetic process of Mn_{SA}/GDY. (b) SEM image of GDY. (c and d) SEM images of Mn_{SA}/GDY at different scale bars. (e) Contact angle measurements of Mn_{SA}/GDY.

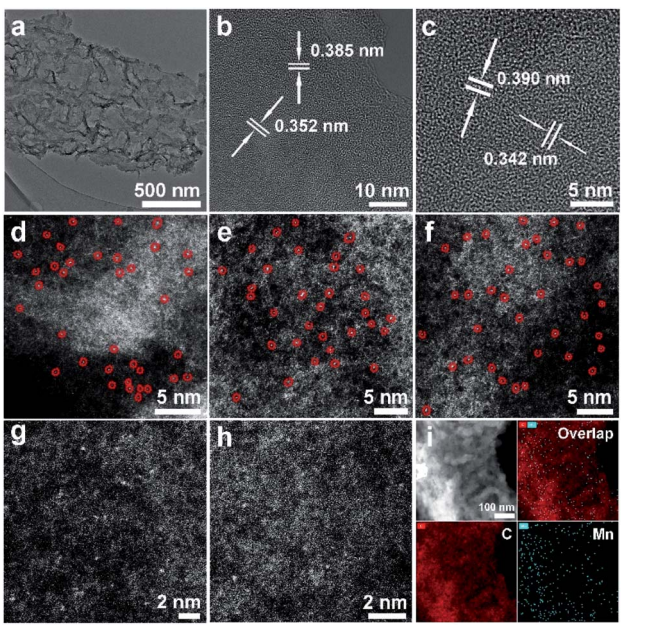

Fig. 2 (a) TEM image of Mn_{SA}/GDY. (b and c) HRTEM images of Mn_{SA}/GDY. (d–h) HAADF images of Mn_{SA}/GDY at different scale bars. (i) STEM image of Mn_{SA}/GDY and corresponding elemental mapping results of Mn_{SA}/GDY.

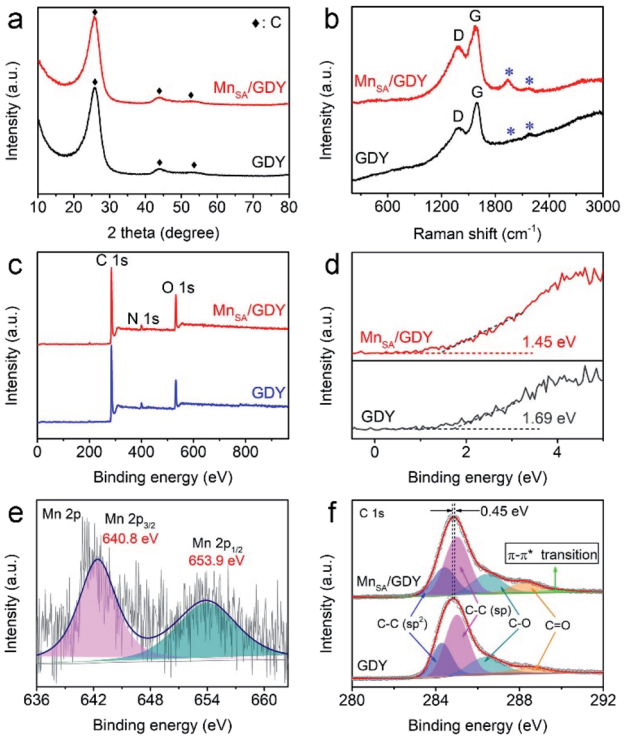

Fig. 3 (a) XRD patterns of Mn_{SA}/GDY and GDY. (b) Raman spectra of Mn_{SA}/GDY and GDY. (c) XPS survey of Mn_{SA}/GDY and GDY. (d) Valence band spectra of Mn_{SA}/GDY and GDY. (e) Mn 2p XPS spectrum of Mn_{SA}/GDY. (f) C 1s XPS spectra of Mn_{SA}/GDY and GDY.

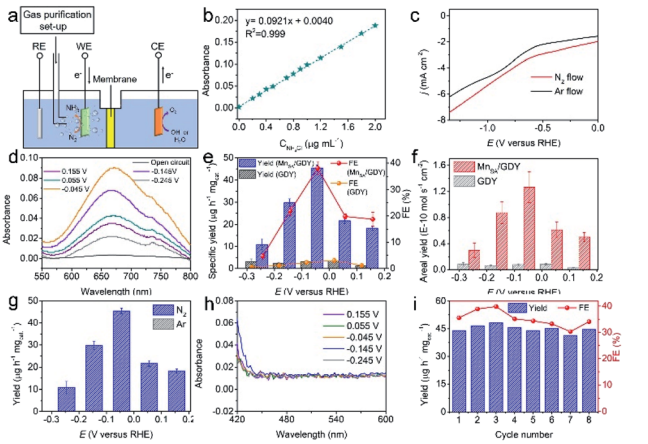

Fig. 4 (a) Schematics of the cell configuration for the NRR under ambient conditions. (b) Calibration curve used for the quantification of produced ammonia. (c) Polarization curves recorded under N_2 and Ar atmospheres. (d) UV-vis spectra of the electrolytes after the NRR at different potentials for 1 h under ambient conditions. (e) Specific ammonia yields and FEs of Mn_{SA}/GDY and pure GDY at different potentials in N_2-saturated 0.1 M Na_2SO_4 (bars present standard deviation). (f) Areal ammonia yields and FEs of Mn_{SA}/GDY and pure GDY at different potentials in N_2-saturated 0.1 M Na_2SO_4 (bars present standard deviation). (g) Y_{NH_3} of Mn_{SA}/GDY obtained at different potentials in Ar- and N_2-saturated 0.1 M Na_2SO_4, respectively (bars present standard deviation). (h) UV-vis spectra for the detection of N_2H_4 on Mn_{SA}/GDY at applied potentials in N_2-saturated 0.1 M Na_2SO_4. (i) Durability test results of Mn_{SA}/GDY at −0.045 V *versus* RHE in 0.1 M Na_2SO_4.

(VBM) of the samples where the VBM of Mn_{SA}/GDY shifted closer to the Fermi level, implying promoted conductivity after anchoring Mn atoms on GDY.[30] Fig. 3e shows the Mn 2p XPS spectrum of Mn_{SA}/GDY with two peaks located at 642.4 eV and 653.9 eV. These peaks correspond to the spin doublet of Mn $2p_{3/2}$ and Mn $2p_{1/2}$ with a separation of 11.5 eV. The fitting of four deconvoluted peaks in the high-resolution Mn $2p_{3/2}$ XPS spectrum given in Fig. S1† indicated the presence of multiple Mn valences.[36,37] The C 1s XPS spectrum of Mn_{SA}/GDY (Fig. 3f) suggested a new sub-peak at 290.0 eV, which was attributed to the π–π* transitions originating from the interactions between the GDY and heterogeneous metal species.[21,22] All these findings confirmed the synergistic effect between individually anchored Mn atoms and the GDY substrate which arises from the unique structural and electronic properties of GDY.

The electrocatalytic nitrogen reduction activities of Mn_{SA}/GDY were evaluated in neutral 0.1 M Na_2SO_4 electrolyte using a gas purification set-up (Fig. 4a). The freshly prepared samples were kept in a glove box filled with Ar to prevent nitrogen compounds and other contaminants in the atmosphere from adsorbing on the surface. The feeding gas was carefully purified through a Cu trap to remove any possible contaminants containing NO_x or other nitrogen species before each test. The polarization curves obtained under N_2 and Ar atmospheres (Fig. 4c) demonstrate the existence of the nitrogen reduction reaction. Fig. 4e and f exhibit the specific and areal ammonia yield (Y_{NH3}) and the corresponding faradaic efficiency (FE) of Mn_{SA}/GDY and GDY at different applied potentials from 0.155 V–0.245 V *versus* RHE, respectively. The corresponding UV-vis absorption curves and chronoamperometry curves are shown in Fig. 4d and S3a,† respectively. It was observed that Mn_{SA}/GDY displayed a higher Y_{NH3} and FE than those of pure GDY. The highest specific Y_{NH3} (45.35 ± 1.38 μg h^{-1} mg$_{cat.}^{-1}$, which could be converted into an areal Y_{NH3} of $(1.27 \pm 0.24) \times 10^{-10}$ mol s^{-1} cm^{-2}) and FE ($38.08 \pm 2.26\%$) for Mn_{SA}/GDY were obtained at −0.045 V *versus* RHE. These results outperform those of most atomic NRR electrocatalysts and even some nano-scale materials (Table S1†).[38–46] Electrochemical reduction reactions were performed under an Ar atmosphere to confirm the nitrogen source of the detected ammonia. No ammonia could be detected when Ar was applied as the feeding gas (Fig. 4g and S4†), verifying that the ammonia detected in the tests originated from the reduction of nitrogen rather than contaminants. UV-vis spectra ranging from 400 to 600 nm of the electrolytes after the NRR were measured to detect the possible N_2H_4 by-product. As shown in Fig. 4h, Mn_{SA}/GDY exhibited 100% selectivity for ammonia production in the absence of the characteristic peak of N_2H_4 at 455 nm at all applied potentials. The durability of the Mn_{SA}/GDY electrocatalyst was evaluated through a cycling test where the NRR was performed for 1 h at −0.045 V *versus* RHE in each cycle. Fig. 4i indicates that the Y_{NH3} and FE of Mn_{SA}/GDY could still be maintained after eight cycles, implying excellent stability. SEM and TEM images shown in Fig. S5† exhibited a well-retained morphological and chemical structure of Mn_{SA}/GDY

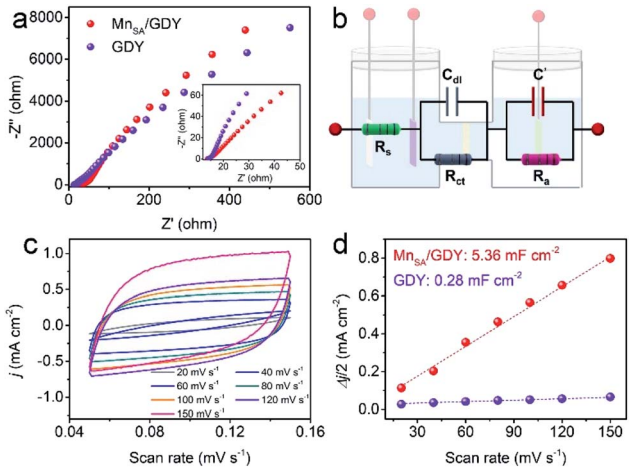

Fig. 5 (a) Electrochemical impedance spectra of Mn$_{SA}$/GDY and GDY (inset: simulated Nyquist plots of Mn$_{SA}$/GDY and GDY). (b) Corresponding fitted equivalent circuit model. (c) CV curves of Mn$_{SA}$/GDY at different scan rates. (d) Estimated C_{dl} values of Mn$_{SA}$/GDY and GDY.

after the durability test verifying the good structural stability of Mn$_{SA}$/GDY during electrochemical measurements.

Electrochemical impedance spectra (EIS) and electrochemically active surface area (ECSA) were measured to determine the intrinsic electrochemical properties of Mn$_{SA}$/GDY. The Nyquist plots of Mn$_{SA}$/GDY and GDY are shown in Fig. 5a, and fitted by an equivalent circuit model (Fig. 5b) comprising the solution resistance (R_s) and charge transfer resistance (R_{ct}). It was observed that both R_s and R_{ct} for Mn$_{SA}$/GDY decreased after the anchoring of Mn atoms on the GDY substrate, as compared to that of pristine GDY. This result indicates the more facilitated electron transfer capability of Mn$_{SA}$/GDY during the NRR. The electrochemical double layer capacitance (C_{dl}) of Mn$_{SA}$/GDY and GDY was measured and is displayed in Fig. 5c and d. The higher C_{dl} of Mn$_{SA}$/GDY suggested its larger ECSA, which could afford more abundant active sites and thus result in its higher reaction efficiency.

We further conducted XPS measurements on Mn$_{SA}$/GDY after cycling stability tests (Fig. S7†). As shown in Fig. S7,† the N 1s XPS spectrum after cycling stability tests could be deconvoluted into two subpeaks corresponding to the N–H bond and absorbed N_2 respectively. This revealed the absorbance of N_2 and ammonia products as well as the corresponding reaction intermediates on the surface of the catalyst. The lower binding energy of the C 1s XPS spectrum of Mn$_{SA}$/GDY after the reaction, as compared to that of as-prepared Mn$_{SA}$/GDY, imply charge transfer from Mn atoms to GDY during the electrocatalysis.

Conclusions

In summary, we have successfully synthesized Mn atomic catalysts supported on a GDY substrate with an atomic mass loading of 0.19 wt%. This Mn$_{SA}$/GDY electrocatalyst exhibits a definite chemical structure, promoted charge transfer capability and abundant active sites. It demonstrates promising performance towards electrocatalytic nitrogen reduction to ammonia, where the ammonia yield and FE could reach up to 46.78 μg h^{-1} mg$_{cat.}^{-1}$ (1.54×10^{-10} mol s^{-1} cm^{-2}) and 39.83%, respectively, and the activity could be retained well after eight cycling tests. These results exceed those of most reported conventional atomic electrocatalysts and heterostructured ones. This work further broadens the application space of GDY-based atomic electrocatalysts and proves their strong competitiveness in the field of catalysis.

Conflicts of interest

There are no conflicts to declare.

Acknowledgements

We acknowledge the support from the National Key Research and Development Project of China (2018YFA0703501), the National Nature Science Foundation of China (21790050, 21790051, and 22021002), and the Key Program of the Chinese Academy of Sciences (QYZDY-SSW-SLH015). We also would like to thank Professor Jun Luo (Tianjin University of Technology, China) for his assistance with the HAADF imaging measurements.

References

1 W. Guo, K. Zhang, Z. Liang, R. Zou and Q. Xu, *Chem. Soc. Rev.*, 2019, **48**, 5658–5716.
2 B. H. R. Suryanto, H. Du, D. Wang, J. Chen, A. N. Simonov and D. R. MacFarlane, *Nat. Catal.*, 2019, **2**, 290–296.
3 X. Guo, H. Du, F. Qu and J. Li, *J. Mater. Chem. A*, 2019, **7**, 3531–3543.
4 G. Qing, R. Ghazfar, S. T. Jackowski, F. Habibzadeh, M. M. Ashtiani, C. Chen, M. R. Smith and T. W. Hamann, *Chem. Rev.*, 2020, **120**, 5437–5516.
5 C. Guo, J. Ran, A. Vasileff and S. Qiao, *Energy Environ. Sci.*, 2018, **11**, 45–56.
6 X. Cui, C. Tang and Q. Zhang, *Adv. Energy Mater.*, 2018, **8**, 1800369.
7 M. A. Shipman and M. D. Symes, *Catal. Today*, 2017, **286**, 57–68.
8 W. Seh Zhi, J. Kibsgaard, F. Dickens Colin, I. Chorkendorff, K. Nørskov Jens and F. Jaramillo Thomas, *Science*, 2017, **355**, eaad4998.
9 M. Shi, D. Bao, S. Li, B. Wulan, J. Yan and Q. Jiang, *Adv. Energy Mater.*, 2018, **8**, 1800124.
10 M. Shi, D. Bao, S. Li, B. Wulan, Y. Li, Y. Zhang, J. Yan and Q. Jiang, *Adv. Mater.*, 2017, **29**, 1606550.
11 H. Shen, C. Choi, J. Masa, X. Li, J. Qiu, Y. Jung and Z. Sun, *Chem*, 2021, **7**, 1708–1754.
12 S. Z. Andersen, V. Čolić, S. Yang, J. A. Schwalbe, A. C. Nielander, J. M. McEnaney, K. Enemark-Rasmussen, J. G. Baker, A. R. Singh, B. A. Rohr, M. J. Statt, S. J. Blair, S. Mezzavilla, J. Kibsgaard, P. C. K. Vesborg, M. Cargnello, S. F. Bent, T. F. Jaramillo, I. E. L. Stephens, J. K. Nørskov and I. Chorkendorff, *Nature*, 2019, **570**, 504–508.

13 X. Li, X. Li, Y. Ma, Q. Wei, W. Qiu, H. Guo, X. Shi, P. Zhang, A. M. Asiri, L. Chen, B. Tang and X. Sun, *Adv. Energy Mater.*, 2018, **8**, 1801357.
14 J. Han, X. Ji, X. Ren, G. Cui, L. Li, F. Xie, H. Wang, B. Li and X. Sun, *J. Mater. Chem. A*, 2018, **6**, 12974–12977.
15 H. Jin, L. Li, X. Liu, C. Tang, W. Xu, S. Chen, L. Song, Y. Zheng and S. Qiao, *Adv. Mater.*, 2019, **31**, 1902709.
16 Y. Fang, Z. Liu, J. Han, Z. Jin, Y. Han, F. Wang, Y. Niu, Y. Wu and Y. Xu, *Adv. Energy Mater.*, 2019, **9**, 1803406.
17 X. Chen, Y. Liu, C. Ma, J. Yu and B. Ding, *J. Mater. Chem. A*, 2019, **7**, 22235–22241.
18 W. Qiu, X. Xie, J. Qiu, W. Fang, R. Liang, X. Ren, X. Ji, G. Cui, A. M. Asiri, G. Cui, B. Tang and X. Sun, *Nat. Commun.*, 2018, **9**, 3485.
19 L. Zhang, L. Ding, G. Chen, X. Yang and H. Wang, *Angew. Chem., Int. Ed.*, 2019, **58**, 2612–2616.
20 Y. Song, D. Johnson, R. Peng, K. Hensley Dale, V. Bonnesen Peter, L. Liang, J. Huang, F. Yang, F. Zhang, R. Qiao, P. Baddorf Arthur, J. Tschaplinski Timothy, L. Engle Nancy, C. Hatzell Marta, Z. Wu, A. Cullen David, M. Meyer Harry, G. Sumpter Bobby and J. Rondinone Adam, *Sci. Adv.*, 2018, **4**, e1700336.
21 G. Li, Y. Li, H. Liu, Y. Guo, Y. Li and D. Zhu, *Chem. Commun.*, 2010, **46**, 3256–3258.
22 Y. Li, L. Xu, H. Liu and Y. Li, *Chem. Soc. Rev.*, 2014, **43**, 2572–2586.
23 Z. Jia, Y. Li, Z. Zuo, H. Liu, C. Huang and Y. Li, *Acc. Chem. Res.*, 2017, **50**, 2470–2478.
24 Y. Xue, B. Huang, Y. Yi, Y. Guo, Z. Zuo, Y. Li, Z. Jia, H. Liu and Y. Li, *Nat. Commun.*, 2018, **9**, 1460.
25 X. Gao, J. Zhou, R. Du, Z. Xie, S. Deng, R. Liu, Z. Liu and J. Zhang, *Adv. Mater.*, 2016, **28**, 168–173.
26 L. Hui, Y. Xue, B. Huang, H. Yu, C. Zhang, D. Zhang, D. Jia, Y. Zhao, Y. Li, H. Liu and Y. Li, *Nat. Commun.*, 2018, **9**, 5309.
27 H. Shang, Z. Zuo, L. Yu, F. Wang, F. He and Y. Li, *Adv. Mater.*, 2018, **30**, 1801459.
28 Y. Fang, Y. Xue, Y. Li, H. Yu, L. Hui, Y. Liu, C. Xing, C. Zhang, D. Zhang, Z. Wang, X. Chen, Y. Gao, B. Huang and Y. Li, *Angew. Chem., Int. Ed.*, 2020, **59**, 13021–13027.
29 Y. Fang, Y. Xue, L. Hui, Y. Yu and Y. Li, *Angew. Chem., Int. Ed.*, 2021, **60**, 3170–3174.
30 L. Hui, Y. Xue, H. Yu, Y. Liu, Y. Fang, C. Xing, B. Huang and Y. Li, *J. Am. Chem. Soc.*, 2019, **141**, 10677–10683.
31 L. Hui, Y. Xue, H. Yu, C. Zhang, B. Huang and Y. Li, *ChemPhysChem*, 2020, **21**, 2145–2149.
32 H. Yu, L. Hui, Y. Xue, Y. Liu, Y. Fang, C. Xing, C. Zhang, D. Zhang, X. Chen, Y. Du, Z. Wang, Y. Gao, B. Huang and Y. Li, *Nano Energy*, 2020, **72**, 104667.
33 H. Yu, Y. Xue, L. Hui, C. Zhang, Y. Fang, Y. Liu, X. Chen, D. Zhang, B. Huang and Y. Li, *Natl. Sci. Rev.*, 2021, **8**, nwaa213.
34 Z. Feng, Y. Tang, W. Chen, Y. Li, R. Li, Y. Ma and X. Dai, *Phys. Chem. Chem. Phys.*, 2020, **22**, 9216–9224.
35 D. Ma, Z. Zeng, L. Liu and Y. Jia, *J. Energy Chem.*, 2021, **54**, 501–509.
36 E. S. Demidov, S. Y. Zubkov, V. P. Lesnikov, G. A. Maksimov, D. E. Nikolichev and V. V. Podol'skii, *J. Surf. Invest.: X-Ray, Synchrotron Neutron Tech.*, 2008, **2**, 541–545.
37 L. M. Ioffe, P. Bosch, T. Viveros, H. Sanchez and Y. G. Borodko, *Mater. Chem. Phys.*, 1997, **51**, 269–275.
38 W. Peng, M. Luo, X. Xu, K. Jiang, M. Peng, D. Chen, T. Chan and Y. Tan, *Adv. Energy Mater.*, 2020, **10**, 2001364.
39 L. Zhang, G. Fan, W. Xu, M. Yu, L. Wang, Z. Yan and F. Cheng, *Chem. Commun.*, 2020, **56**, 11957–11960.
40 X. Wang, D. Wu, S. Liu, J. Zhang, X. Fu and J. Luo, *Nano-Micro Lett.*, 2021, **13**, 125.
41 Y. Li, J. Li, J. Huang, J. Chen, Y. Kong, B. Yang, Z. Li, L. Lei, G. Chai, Z. Wen, L. Dai and Y. Hou, *Angew. Chem., Int. Ed.*, 2021, **60**, 9078–9085.
42 B. Yu, H. Li, J. White, S. Donne, J. Yi, S. Xi, Y. Fu, G. Henkelman, H. Yu, Z. Chen and T. Ma, *Adv. Funct. Mater.*, 2020, **30**, 1905665.
43 N. Cao, Z. Chen, K. Zang, J. Xu, J. Zhong, J. Luo, X. Xu and G. Zheng, *Nat. Commun.*, 2019, **10**, 2877.
44 Q. Qin, Y. Zhao, M. Schmallegger, T. Heil, J. Schmidt, R. Walczak, G. Gescheidt-Demner, H. Jiao and M. Oschatz, *Angew. Chem., Int. Ed.*, 2019, **58**, 13101–13106.
45 Y. Tong, H. Guo, D. Liu, X. Yan, P. Su, J. Liang, S. Zhou, J. Liu, G. Lu and S. Dou, *Angew. Chem., Int. Ed.*, 2020, **59**, 7356–7361.
46 Y. Lin, S. Zhang, Z. Xue, J. Zhang, H. Su, T. Zhao, G. Zhai, X. Li, M. Antonietti and J. Chen, *Nat. Commun.*, 2019, **10**, 4380.